Fatigue life determination based on infrared thermographic data for MultiDirectional (MD) CFRP composite laminates

Zijiao Jia, Marie-Laetitia Pastor, Christian Garnier, Xiaojing Gong

Version of Record: https://www.sciencedirect.com/science/article/pii/S0263822323005469
Manuscript_4d0e4695a3496f62dc9585a7c7114f56

Fatigue life determination based on infrared thermographic data for MultiDirectional (MD) CFRP composite laminates

Zijiao Jia[a,b], Marie-Laetitia Pastor[a*], Christian Garnier[b], Xiaojing Gong[a]

[a] *Institut Clément Ader (ICA), CNRS, UMR 5312, Univ. Toulouse, UPS, 1 rue Lautréamont, 65000 Tarbes, France.*

[b] *INP-ENIT, LGP, Univ. Toulouse, 47 avenue d'Azereix, F-65016 Tarbes, France.*

Abstract: Infrared thermography is a useful tool for the rapid determination of fatigue properties. A previously proposed fatigue life model, which combines the stiffness degradation $k(N)$ with thermographic data ΔT_{stab}, has been successfully applied to UD and ±45° CFRP laminates. In view of more complex damage mechanisms in multidirectional laminates, the model is modified in this work to overcome the conservative predictions. The S-N curves determined by the modified model are compared with the experimental results of traditional fatigue tests on Quasi-Isotropic (QI) and cross-ply CFRP laminates. Very good consistency was observed. In particular, the S-N curve corresponding to fatigue life of $N_{fl} = 10^6$ cycles is conservative compared to that from the traditional fatigue test results, but the maximum safety factors are no more than 1.15 and 1.08 for QI and cross-ply laminates, respectively. Both S-N curves corresponding to $N_{fl} = 10^7$ cycles for two tested laminates lie within the 95% confidence interval of traditional experimental results. Therefore, based on infrared thermographic data, the modified model proposed in this study is more general. It allows to determine the S-N curves of QI and cross-ply CFRP laminates just in about ten hours of testing machine time instead of one month and a half using traditional fatigue tests, even though more experimental data (other types of MD stacking sequences, composite materials, under other fatigue modes, etc.) are necessary to demonstrate the applicability of modified model to all types of MD laminates.

Keywords: Multidirectional CFRP laminates, fatigue life, infrared thermography, damage accumulation, 3 parameter model

1 Introduction

The application of Carbon Fiber Reinforced Plastics (CFRP) as a high-performance engineering material is becoming widespread owing to their excellent specific stiffness and strength, corrosion and creep resistance [1], etc. In service, fatigue degradation caused by repeated cyclic loading is recognized as a common mode of failure for the CFRP structures. As a consequence, there have been extensive studies investigating the fatigue properties of CFRP materials [2-5] . Most of these studies were based on measuring the number of cycles to failure at different stress levels with an intention of generating the S-N curves. This is particularly costly and time-consuming. Besides, for a given material, its fatigue properties can depend on different parameters, such as loading frequencies, stress ratios, geometrical shapes and dimensions, manufacturing processes and surface roughness, etc. [6-9]. Moreover,

* Corresponding author: Marie-Laetitia Pastor
E-mail address: marie.laetitia.pastor@iut-tarbes.fr

in comparison with metals, the fatigue behavior of CFRP is considerably more complicated due to their inherent anisotropy and heterogeneity. Fiber orientation and content [10][11], stacking sequence [12][13], fiber/matrix interface quality [14][15], etc. can all have an influence on their fatigue properties. Therefore, there is a strong need for new approaches to rapidly evaluate the fatigue properties of CFRP. Studies show that the Non Destructive Testing (NDT) methods may satisfy this requirement [16]-[18].

Fatigue of materials is an irreversible energy dissipation process accompanied by temperature variation. InfraRed Thermography (IRT) enables the visible identification of the surface temperature field of a material when it is subjected to mechanical loading. It can be applied not only to access the damage initiation and propagation in real time, but also, based on the thermographic analysis, to predict in a short time fatigue properties (fatigue limit, fatigue life) [18-24]. For example, Risitano et al. firstly developed an empirical method, i.e., One-Curve Method (OCM), to evaluate the fatigue limit and construct the S-N curve of metallic materials [25][26]. Based on the detection of occurrence of intrinsic dissipation energy, Luong et al. put forward a Two-Curve Methodology (TCM) to rapidly determine the fatigue limit of metals [27][28]. Later, the method has been used for the evaluation of fatigue limit of ±45° Glass Fiber Reinforced Plastics (GFRP) [29], UD, ±45° and braided CFRP [30][31]. In the study of Jiang et al. [32], the total plastic-strain-energy density was employed to establish the fatigue failure criterion. They showed that the temperature index, defined as the temperature difference between initial and steady stage, can be used to predict the fatigue life of two superalloys. Amiri et al. [33] pointed out that the initial slope of temperature rise plotted as a function of fatigue cycles could be utilized as an index for fatigue life prediction. On this basis, an approach has been developed to evaluate the fatigue life of aluminum and steel, and an improved method for braided GFRP [34].

However, to the author's knowledge, there are few studies which utilize IRT to determine the fatigue properties of MultiDirectional (MD) composite laminates, probably due to the notably more complicated damage mechanisms in these materials. Besides, as these thermographic methods were originally designed for the metallic materials, they should not be applicable anymore for the MD composite laminates without modification or adaptation.

The damage mechanisms of composite materials under fatigue loading are very complex. But thanks to NDT methods, such as Ultrasonic Scanning (US), Acoustic Emissions (AE), Digital Image Correlation (DIC), etc., it makes it easier to understand and analyze the damage mechanisms [16][17]. According to numerous studies, it is believed that three distinctive stages of damage evolution in composite structures under fatigue loading can be generally distinguished: matrix cracking and fiber-matrix debonding at the beginning of fatigue life, followed by delamination, growth and coalescence of matrix cracks, and fiber fractures in the final stage [35][36]. The accumulation of damages is accompanied with the degradation of stiffness [37][38]. Therefore, measurement of residual stiffness could be used as an indication of the extent of accumulated damages during fatigue loading and further give predictions of fatigue life [39-[43].

In a previous work, a fatigue life model based on stiffness degradation was proposed by Huang et al. [44] by combining the IRT data with damage accumulation process. The proposed method allows to determine S-N curve just in about ten hours of machine time. The model has been successfully applied to determine the fatigue S-N curves of triaxially braided,

unidirectional (UD) [44] and ±45° [45] CFRP laminates.

In this work, firstly Huang's model has been applied to Quasi-Isotropic (QI) CFRP laminates. Nevertheless, it produces rather conservative fatigue life predictions because in a MD laminate, damage initiation and accumulation process are more complex. Hence, secondly the model is modified in the present study. Herein, a new parameter r is introduced into the original Huang's model to consider the influence of more complex damage mechanisms in MD CFRP laminates. A normalization process is proposed for stabilized temperature rise ΔT_{stab} to facilitate the comparison between different specimens. The determination of the parameters of new model has been discussed. This model is first applied to QI CFRP laminates, and then to cross-ply CFRP laminates. A good agreement was found between the S-N curves determined by the proposed model and the experimental results from traditional tests. The modified model is demonstrated to be more general than Huang's model and more reliable for the rapid determination of fatigue life of QI and cross-ply CFRP.

2 Materials and experimental details

The preparation of specimens and detailed experimental procedure are described in this section.

2.1 Materials and specimens

The tested composite laminates were prepared from high strength unidirectional carbon prepreg which is made of HexPly®M79 matrix and carbon fiber (38%/UD150/CHS). Two different multidirectional stacking sequences have been considered for the study: one is cross-ply of $[(0/90)_2/0/(90/0)_2]$, the other one is QI of $[0/45/90/-45]_s$. The laminates were first hand laid up, and then cured in an autoclave at 2.0 bar and at 80 °C for 360 min and were subsequently cooled down to the room temperature under pressure, which resulted in a nominal thickness of 1.204 mm (± 0.018) and 1.009 mm (± 0.025), respectively. The specimens were water-jet cut from the fabricated composite laminates to the dimensions given in Fig. 1, in accordance with ISO 527-4: 2021 [46]. The main advantage of using water-jet cutting is that the cuts made by waterjets are significantly more accurate and precise than those made by other tools (the accuracy is close as 0.001" (0.025 mm)) [47]. Besides, since flow waterjets cut the specimens by erosive action rather than friction and shearing, they produce a uniform smooth edge free of frayed or delaminated areas. This point is rather important because the fatigue property of composite material is significantly affected by the edge quality [48]. To prevent rupture and slippage in the grip region of the test device, glued end-tabs were used at either end of the specimens [49][50]. 1 mm thick and 50 mm long glass fiber reinforced epoxy tabs were adhered to the specimens using Hysol EA 9394 Part A + B epoxy adhesive. The fibers in the tabs were oriented in the ±45° direction.

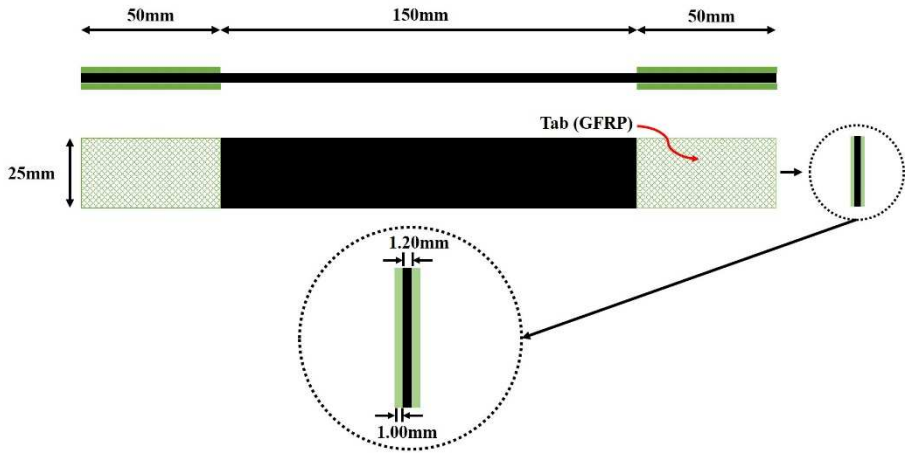

Fig. 1 Dimensions of cross-ply specimens used for the tensile and fatigue tests

2.2 Static tensile tests

To determine the Ultimate Tensile Strength (UTS), quasi-static tensile tests were conducted at room temperature using INSTRON universal testing machine (INSTRON 5500R), equipped with a 100 KN load cell. The experimental setup was shown in Fig. 2 (a). The tests were performed according to standard ISO 527-4: 2021 [46], with a 2.0 mm/min cross-head speed. To ensure repeatability, 3 specimens with identical dimensions were tested for each stacking sequence. During the tests, the tensile force was recorded by the sensor of Instron 5500R testing machine and the tensile strain was measured with a DIC system Aramis 2M (GOM, Braunschweig, Germany). Two 8-bits Complementary Metal Oxide Semiconductor (CMOS) cameras with a resolution of 1624*1236 pixels were positioned on the same side of the specimen to capture the images of the specimen surface. A random speckle pattern which was created by the black and white spray paints was applied on the surface of the specimen prior to the testing. The data recording rate is one frame per second and the post-processing of the obtained results was performed by the Aramis software.

According to the results of static tensile tests, the UTS was determined as 607.5 ± 22.1 MPa and 1329.4 ± 24.7 MPa for the QI and cross-ply laminates, respectively.

2.3 Fatigue tensile tests

The uniaxial tensile fatigue tests were carried out in the servo-hydraulic Instron loading machine, in accordance with the standard ASTM D3479 [49]. The fatigue tests were performed at room temperature in a load amplitude control mode at a frequency of 5Hz and with a stress ratio of $R=0.1$.

Traditional fatigue tests were conducted with various stress levels, at least three tests were conducted at each stress level in order to produce a reliable S-N curve. Each test was stopped at specimen's failure or until a run-out of 10^6 cycles was reached.

In addition, step-loading fatigue tests monitored by infrared camera were also performed to obtain the thermographic data for the rapid fatigue life prediction. The maximum stress amplitude of the cyclic loading started from 30% UTS. A loading step of 5% UTS was used until the failure of the specimen. For each loading level, the specimen is only tested for 6000 cycles, which were sufficient to produce a stabilized temperature rise. A FLIR X6800sc Series IR camera was utilized to measure the surface temperature of the specimen in situ and in real

time. The device used in this work was a mid-wavelength InfraRed camera, with a spectrum response covering the wavelengths ranging from 3 to 5 μm. The detector spatial resolution was 640×512 pixels and the thermal sensitivity was 18 mK at 30 °C. The frame rate speed was set as 520 Hz. To increase the thermal emissivity of the specimen surface, before fatigue testing, the surface of the specimen was coated with a thin layer of black mat paint. The detailed experimental setup is depicted in Fig. 2 (b). A reference specimen is placed nearby the testing specimen to monitor the temperature change of ambient environment. Three specimens were tested for each stacking sequence. The experimental stiffness *K(N)*, defined as the slope of the force-displacement hysteresis loops, was recorded at fixed time intervals of the fatigue life, as presented in Fig. 3.

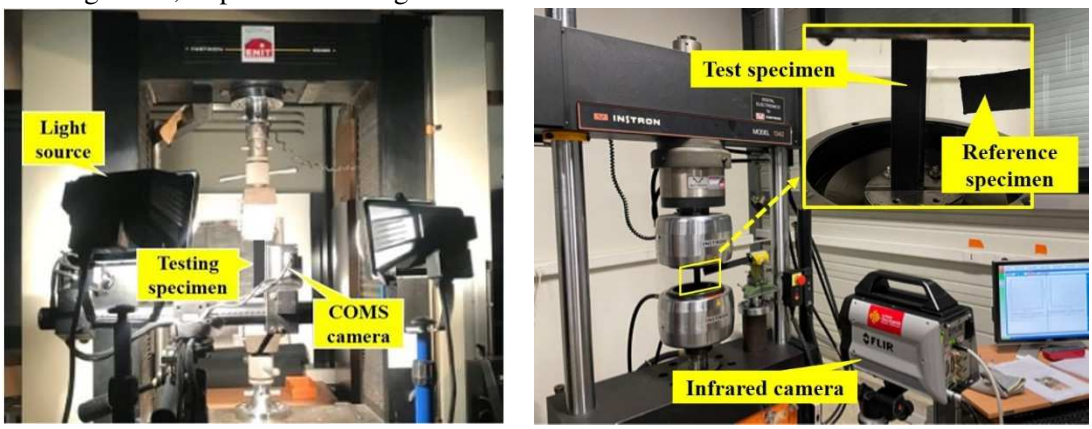

(a) (b)

Fig. 2. Experimental setup: (a) static tensile tests; (b) fatigue tests with the use of IR camera

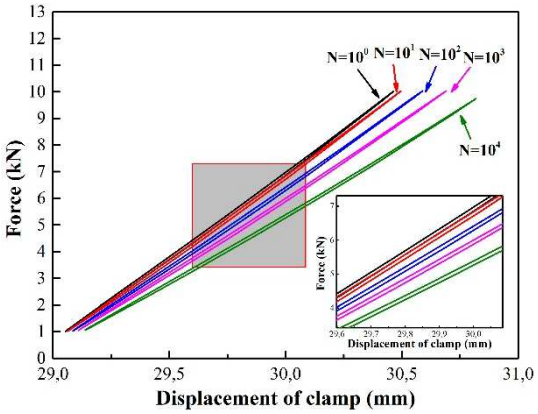

Fig. 3. Typical hysteresis loop during fatigue tests (unit of N: cycles)

3 Fatigue life prediction based on thermographic data

In this section, the fatigue life model proposed by Huang is first reviewed and applied to the data of QI laminates. The S-N curves determined by Huang's model are found to be much lower than the traditional fatigue test results. Therefore, the model was modified. Thereafter, the experimental data of both QI and cross-ply laminates will be used to validate the model.

3.1 Huang's model [44]

The evolution of accumulative damage as a function of the number of fatigue loading cycles may be generally described by the curve in Fig. 4. Three distinctive stages are shown in this figure [39]. In the first stage, rapid development of damages is attributed to the formation of

micro-cracks in the matrix and/or in the fiber-matrix interfaces. The second stage, which occupies the majority (70-80%) of the fatigue lifetime [53], is characterized by delamination propagation and the growth and coalescence of matrix cracks [54]. Finally, in the third stage, an accelerated damage growth caused by the fracture of fibers leads to the final failure of laminates [55][56]. The accumulation of damages causes the stiffness degradation which can also be divided in three distinctive stages (Fig. 4).

Therefore, in the work of Huang et al. [44], the change in residual stiffness has been used to express the extent of accumulated damages in the material. The damage variable *D* is defined as [57]:

$$D(N) = \frac{1 - k(N)}{1 - k_f} \tag{1}$$

Where *N* is the number of loading cycles, $k(N)$ and k_f, defined as $K(N)/K_0$ and K_f/K_0, are the normalized residual stiffnesses at Nth cycle and at the end of second stage (N_f), respectively. K_0 is the initial stiffness.

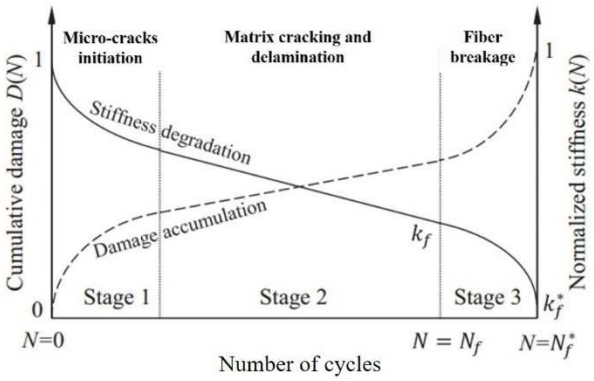

Fig. 4. A typical trend for stiffness degradation and damage accumulation during fatigue loading [56]

Huang et al. [44] assumed that the normalized stiffness $k(N)$ is associated with the stabilized temperature rise ΔT_{stab} by Eq. (2):

$$k(N) = 1 - p'\Delta T_{stab} N^{1/q} \; with \; q \geq 1 \tag{2}$$

Where *p'* and *q* are two material constants, independent of temperature and loading cycles.

Substituting Eq. (2) into Eq. (1) and considering the boundary condition that as the number of cycles approaches the fatigue life N_f, *D* approaches 1, Eq. (1) becomes:

$$1 = \frac{p'\Delta T_{stab} {N_f}^{1/q}}{1 - k_f} \; with \; q \geq 1 \tag{3}$$

This formula can be expressed in another form:

$$N_f = \left(\frac{1 - k_f}{p'\Delta T_{stab}(\sigma)}\right)^q \; with \; q \geq 1 \tag{4}$$

Eq. (4) can be used to determine the fatigue life of CFRP once the values of *p'*, *q* and the relationship between stabilized temperature rise and maximum loading stress are known.

3.2 Application of the model proposed by Huang et al. [44]

In this section, Huang's model [44] is applied to the experimental data of QI CFRP laminates

to validate model's generalization (Fig. 5).

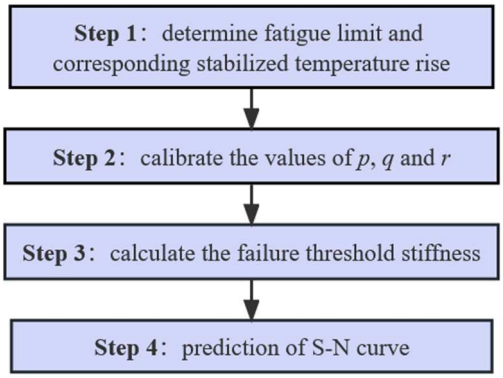

Fig. 5 Flowchart of fatigue life determination

In the first step, the method proposed in Jia's work [58]was adopted to evaluate the fatigue limit. This method has been proven to be an efficient approach for the fatigue limit determination of MD composite laminates. The fatigue limit is determined as 65% UTS (Fig. 6(a)) and the corresponding stabilized temperature rise as 4.205°C, as shown in Fig. 6 (b). In the second step, Eq. (2) is employed to fit the data of normalized stiffness degradation (maximum stress of 50%, 55%, 60%, 65% and 70% UTS) as a function of the number of loading cycles and stabilized temperature rise using 3D surface fitting with help of a MATLAB program. The best fit values of p' and q are determined as 2.344e^{-2} ($°C \times Cycle^{1/q})^{-1}$ and 11.80, respectively. The corresponding coefficient of determination R^2 is 0.884. The failure threshold stiffnesses k_f corresponding to a fatigue life N_{fl} of 10^6 and 10^7 cycles are evaluated as 0.682 and 0.614 in the third step, respectively.

Having the values of p', q and k_f, the whole S-N curve can be determined in the fourth step and a plot of the prediction curve is shown in Fig. 7. Traditional fatigue test results with 95% confidence interval are also included in the plot for comparison. As can be seen from this figure, the S-N curves corresponding to $N_{fl} = 10^6$ cycles and $N_{fl} = 10^7$ cycles are both below the 95% confidence interval. The determined fatigue life is much lower than the traditional fatigue test results overall. The error, defined as ((95% confidence interval-Huang's model)/95% confidence interval), between the maximum stress obtained from the S-N curve corresponding to $N_{fl} = 10^6$ cycles and the lower boundaries of 95% confidence interval varies between 93.82% and 98.39%, while for the S-N curve corresponding to $N_{fl} = 10^7$ cycles, the error ranges from 38.24% to 83.87%. In conclusion, the fatigue life of the tested QI CFRP laminates determined by Huang's model is too conservative to be accepted.

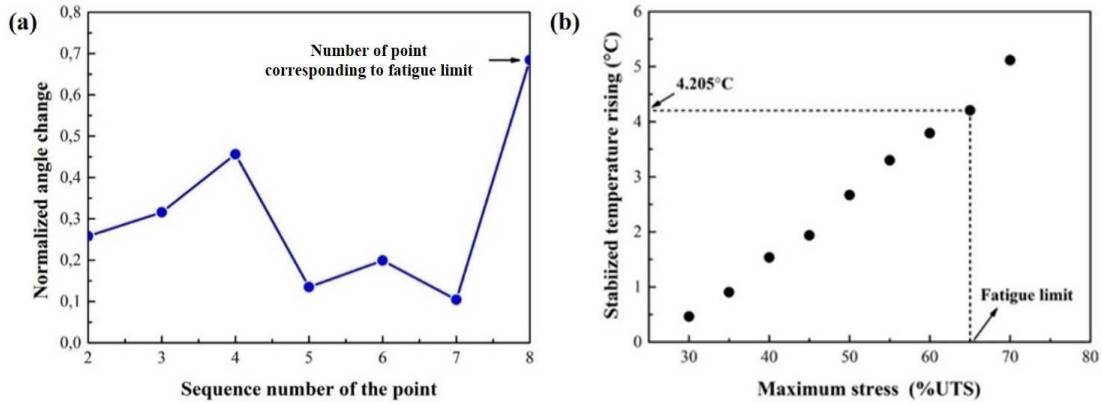

Fig. 6. Fatigue limit determination of QI laminates: (a) loci of normalized angle change vs sequence number of the point; (b) stabilized temperature rise vs maximum stress.

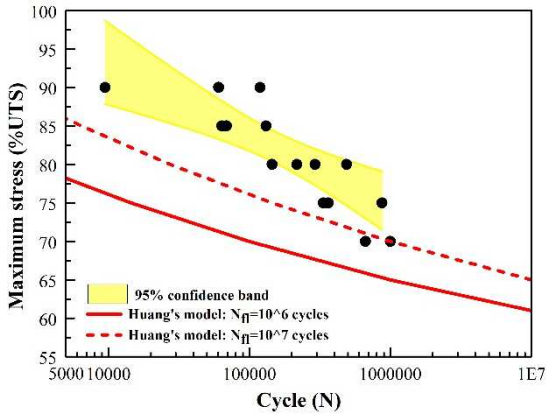

Fig. 7. Comparison of determined S-N curves by Huang's model with traditional fatigue test results for QI laminates

3.3 Proposition of modified model

Recall that Huang's model has been applied successfully to UD [44] and ±45° laminates [45] made from the same prepreg as that used in this study. But it underestimates the fatigue life of QI laminates. In fact, according to the study of Huang et al. [44], in Eq. (2), the parameter *p'* allows to regulate the scale of temperature rise, while the role of *q* is to control the shape of the function. For a MD laminate under tensile loading, each ply with different fiber orientation can be subjected to different stresses leading to more complex damage modes compared to that of UD and ±45° laminates. The differences in damage mechanisms are reflected in the relationship between the normalized stiffness and the stabilized temperature rise. In Huang's model, when the values of *p'*, *q* and *N* are determined, the Eq. (2) becomes $k(N) = 1 - p'\Delta T_{stab}(\sigma)N^{1/q} = 1 - s \times \Delta T_{stab}(\sigma)\ with\ q \geq 1$ (*s* is a constant). As can be seen from the equation, there is a linear decrease of stiffness with the increase of stabilized temperature rise. The experimental stiffness degradation data plotted as a function of stabilized temperature rise of specimens with different stacking sequence when the number of loading cycles equals to 4000 and 8000 cycles are illustrated in Fig. 8 and Fig. 9. The values of these two numbers of loading cycles are chosen arbitrarily. For the UD (or for ± 45°) laminates, according to the study of Huang et al. [44][45], the best-fit values of *p'* and *q* are $10.87 \times 10^{-2}(°C \times cycle^{1/q})^{-1}$ ($1.68 \times 10^{-3}(°C \times cycle^{1/q})^{-1}$) and 4.75 (5.56), respectively. When the values of *N* are taken as 4000 and 8000, the corresponding values of *s* become 0.623 (7.47×10^{-3}) $°C^{-1}$ and 0.721 (8.46×10^{-3}) $°C^{-1}$ and the exact expression for $k(N)$ will change to $k(4000) = 1 - 0.623 \times \Delta T_{stab}(\sigma)$ and $k(8000) = 1 - 0.721 \times \Delta T_{stab}(\sigma)$, respectively. Subsequently, these two linear equations are adopted to fit the experimental data, as shown in Fig. 8. The coefficients of determination R^2 are determined as 0.922 (0.950) and 0.965 (0.9745) when N=4000 cycles and 8000 cycles, respectively, which indicates that the fitting curve agrees well with the experimental data. For the QI laminates, the values of *p'* and *q* determined by Huang's model are 2.344e-2$(°C \times Cycle^{1/q})^{-1}$ and 11.80, respectively. When the number of cycles is equal to 4000 and 8000 cycles, the corresponding values of *s* turn out to be 4.73×10^{-2} $°C^{-1}$ and 5.02×10^{-2} $°C^{-1}$, respectively. The fitting results using these two linear equations for the experimental data are

depicted in Fig. 9. The corresponding R^2 are 0.806 and 0.827, respectively. Based on these R^2 values, it is clear that linear fitting is less accurate for QI laminates.

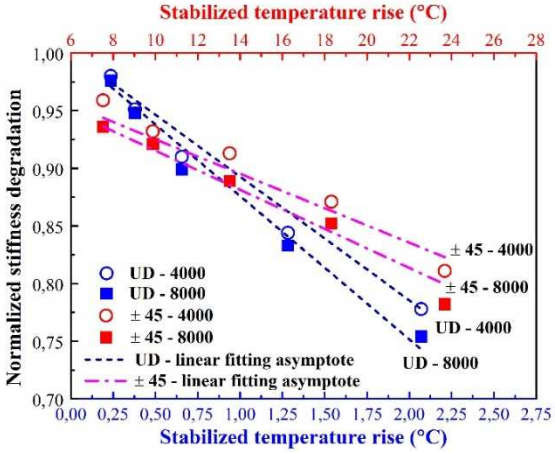

Fig. 8. Normalized stiffness degradation vs stabilized temperature rise for UD and ± 45°laminates (Data from [44] and [45])

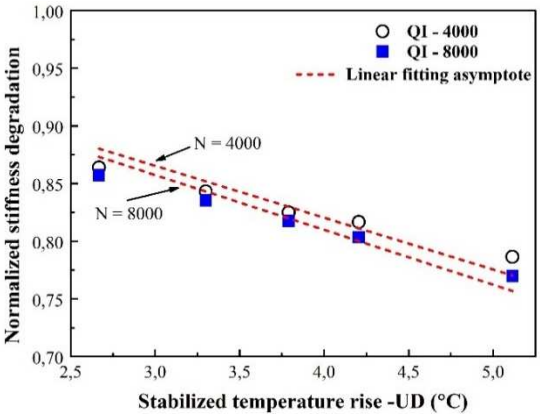

Fig. 9. Normalized stiffness degradation vs stabilized temperature rise for QI laminates

In order to take into account of the complex damage mechanisms in MD laminates, the expression of normalized stiffness $k(N)$ in Eq. (2) can be modified by introducing another parameter *r* as follow:

$$k(N) = 1 - p'\Delta T_{stab}^{r} N^{1/q} \; with \; q \geq 1 \quad (5)$$

However, it should be noted that if the parameter *r* is close to 1, this model returns to the model expressed by Eq. (2). Therefore, the modified model in Eq. (7) is more general and it includes the model in Eq. (2).

In addition, as can be seen from Fig. 8 and Fig. 9, the scale of stabilized temperature rise of different stacking sequences varies deeply from each other. For example, the stabilized temperature rise of UD laminates varies between 0.25 and 2.1°C, while that of $\pm 45°$ laminates ranges from 7 to 24°C. For the ease of comparison between different specimens, a normalization process is proposed for ΔT_{stab}:

$$\Delta T_{stab}^{*} = \Delta T_{stab} / (\Delta T_{stab})_{max} \quad (6)$$

Where ΔT_{stab}^{*} is the normalized stabilized temperature rise, $(\Delta T_{stab})_{max}$ is the maximum value of stabilized temperature rise of each specimen.

Substituting Eq. (6) into Eq. (5), it can be obtained:

$$k(N) = 1 - p(\Delta T^*_{stab})^r N^{1/q} \; with \; q \geq 1 \quad (7)$$

Where $p = p' \times (\Delta T_{stab})^r_{max}$.

Now there are three parameters *p, q* and *r* to determine empirically. The value of these three parameters can be calibrated by fitting experimental data with the help of MATLAB.

3.4 Validation of proposed model

In this section, the experimental data of QI CFRP laminates is first employed to validate the proposed model. Thereafter, the proposed model will be applied to the cross-ply laminates to further demonstrate the universality of this model in the fatigue life prediction of MD laminates.

3.4.1 Case one: QI CFRP laminates

In the first step, as previously mentioned, the fatigue limit and corresponding stabilized temperature rise are determined as 65% UTS and 4.205°C, respectively. In the second step, Eq. (7) is employed to fit the experimental data using MATLAB software. The values of *p*, *q* and *r* were determined as 3.736e-2, 11.776 and 0.660, respectively. The corresponding coefficient of determination R^2 is 0.980. In the third step, according to Eq. (7), the failure threshold stiffness k_f was computed as 0.689 and 0.621 when $N_{fl} = 10^6$ cycles and 10^7 cycles, respectively. Finally, the S-N curves determined using proposed model are illustrated in Fig. 10.Traditional test results with 95% confidence interval and that determined by Huang's model are also plotted in the same figure for comparison.

From Fig. 10, it is found that, compared to the S-N curves determined by Huang's model, those determined by the modified model are obviously closer to the 95% confidence interval for the maximum stress above 65% UTS. The S-N curve corresponding to fatigue life of $N_{fl} = 10^6$ cycles based on proposed model is still lower than the traditional fatigue test results overall. The Safety Factor (SF), defined as the ratio between maximum stress of traditional fatigue tests and that determined by proposed model for a given number of fatigue cycle ($SF = \sigma_{test,N=N_c}/\sigma_{model,N=N_c}$, where N_c is the number of fatigue cycle), lies between 1.09 and 1.15. Both values are very close to 1. On the contrary, the S-N curve corresponding to $N_{fl} = 10^7$ cycles matches well with the traditional fatigue test results. The determined fatigue lives fall totally within the confidence interval. This suggests that in comparison to Huang's model, the modified model is more reliable and promising in predicting the fatigue life of QI CFRP laminates.

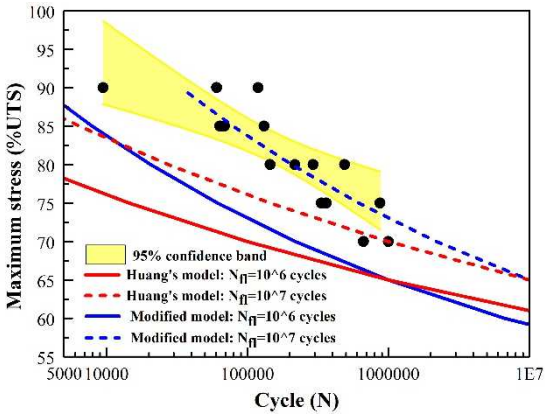

Fig. 10. Comparison of determined S-N curves by two models with traditional fatigue test results

3.4.2 Case two: Cross-ply CFRP laminates

The specific procedure for the prediction of fatigue life of cross-ply laminates based on the proposed model is shown step by step as follows:

Step 1: determine fatigue limit and corresponding stabilized temperature rise based on thermographic data.

Fig. 11 illustrates the average surface temperature rising versus the number of loading cycles under 9 successive stress levels. As can be seen from this figure, for the stress levels from 30% to 70% UTS, the profile reached temperature stabilization after certain loading cycles. It should be noted that the stabilization section for 70% UTS is very short because it is prior to failure. Fig. 12 (a) depicts the normalized angle change plotted as a function of the measured point's number. Similar to the previous case, the new fatigue limit determination approach [57] was employed here and the fatigue limit was determined as 65% UTS (Fig. 12 (b)), which lies favorably with the results obtained by the traditional fatigue tests (68.94% UTS). The corresponding stabilized temperature rise (ΔT_{stab_fl}) is 2.725° C.

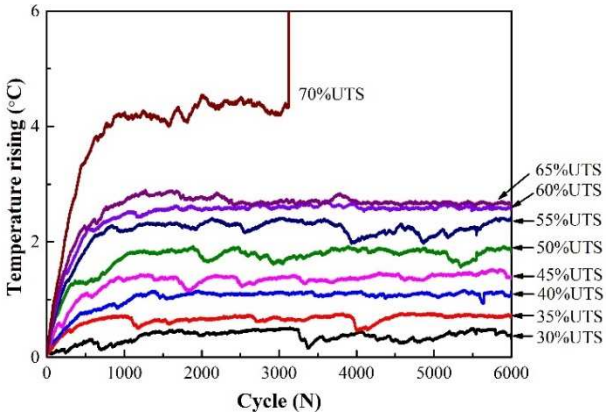

Fig. 11. Temperature evolution vs number of cycles for one cross-ply laminate

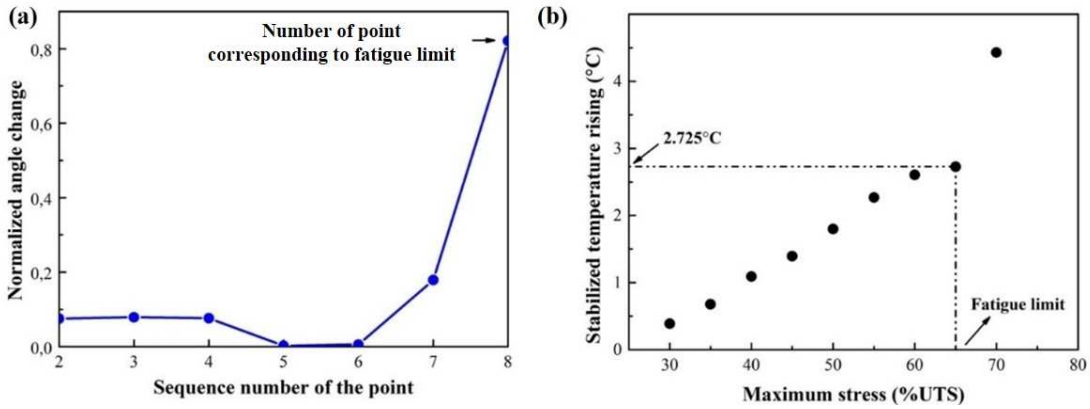

Fig. 12. Fatigue limit determination of cross-ply laminates: (a) loci of normalized angle change vs sequence number of the point; (b) stabilized temperature rise vs maximum stress

Step 2: calibrate the values of p, q and r

A plot of normalized stiffness degradation against the number of loading cycles and normalized stabilized temperature rises under stress level of 45, 50, 55, 60 and 65% UTS are shown in Fig. 13. For each curve, 20 points are sampled, which varies between 0 and 10000 cycles with interval of 500 cycles. A total number of 100 points are used for fitting. Eq. (7) is

adopted to fit the experimental data using MATLAB 3D surface fitting Toolbox to calibrate the value of parameters p, q and r. As shown in Fig. 13, the translucent blue surface is the result of surface fitting of Eq. (7) by MATLAB program. The best-fit values of p, q and r were determined as 8.301e-3, 7.023 and 1.26, respectively.

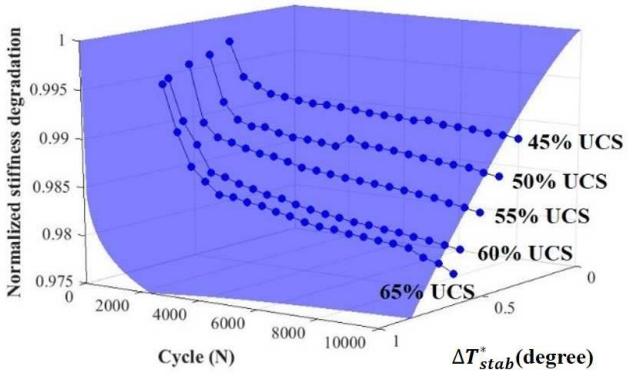

Fig. 13. Surface fitting of Eq. (7) by MATLAB

Step 3: calculate the failure threshold stiffness

Similar to the case of QI laminates, both $k_f(N_{fl} = 10^6$ cycles) and $k_f(N_{fl} = 10^7$ cycles) were chosen for the calculation of failure threshold stiffness. According to Eq. (5), $k_f = 0.955$ when $N_{fl} = 10^6$ cycles while this value is 0.938 when $N_{fl} = 10^7$ cycles.

Step 4: prediction of the S-N curve

The S-N curves calculated using the model proposed in this study are compared with traditional fatigue test results with 95% confidence interval in Fig. 14. It can be clearly seen that the S-N curve corresponding to $N_{fl} = 10^6$ cycles is relatively conservative. The determined fatigue life is lower than the traditional fatigue test results. The SF lies between 1.04 and 1.08. Both are very close to 1. In consideration of the variability of the fatigue test results, this is acceptable. The S-N curve corresponding to $N_{fl} = 10^7$ cycles lies totally within the 95% confidence interval. The error induced by the determined S-N curve ($N_{fl} = 10^7$ cycles) is well within the measurement uncertainty. This approves that the proposed model should be reliable to predict the fatigue life of MD CFRP laminates.

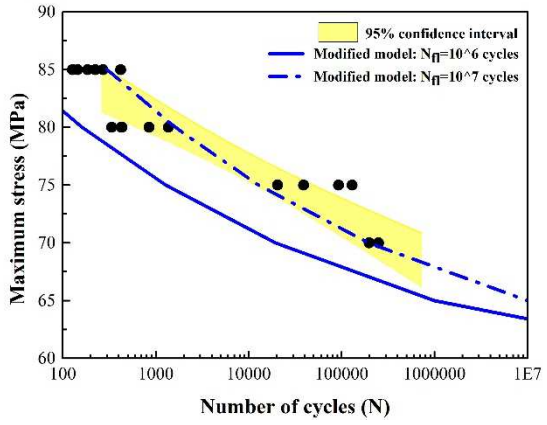

Fig. 14. Comparison of determined S-N curves with traditional fatigue test results for cross-ply laminates

4 Discussions

4.1 Fracture surface observations

Fig. 15 depicts the fracture surfaces of a typical specimen under static tensile loading for each laminate. For the QI laminates, it is shown that transversal detachment of adjacent fibers occurred in 90° and ±45° layers, fiber fracture was detected in ±45° and 0° layers and fiber pull-out could be found in the surface 0° layers [51]. While in the cross-ply laminates, the fracture mode is characterized by a mixture of fiber fracture in the 0° layers along with transversal fiber/matrix debonding in the 90° layers [52]. Besides, delamination can also be found in the interfaces for both two stacking sequences.

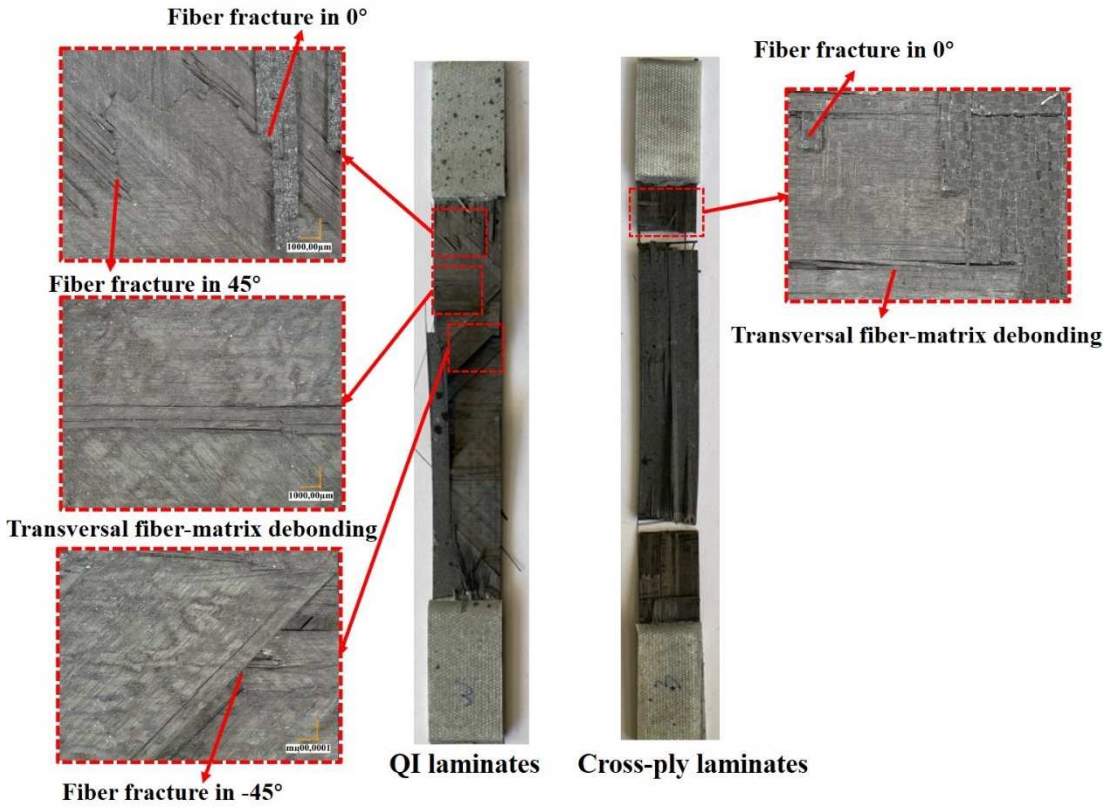

Fig. 15 Observation on fracture surfaces of the specimens under static tensile loading

The fracture surfaces of typical specimens after two kinds of fatigue tests are presented in Fig. 16. Since the damage morphologies of specimens tested under different stress levels are quite identical, therefore, only one specimen is taken here as an example. It can be noticed that there is barely no difference in fracture surfaces between the traditional fatigue test specimens and those who have been subjected to step-loading procedure using IRT. But obviously, the damages in the latter ones are less than the former.

Overall, the failure mode of tension fatigue test specimens is identical with static tensile test specimens except that the fiber fracture in the interior -45° layers was not observed in the fatigue test specimens. However, compared to the static tensile specimens, longer testing duration below the UTS promotes the accumulation of damages, therefore, more delamination can be found between two layers and significantly more fiber pull-out can be found in the surface 0° layers.

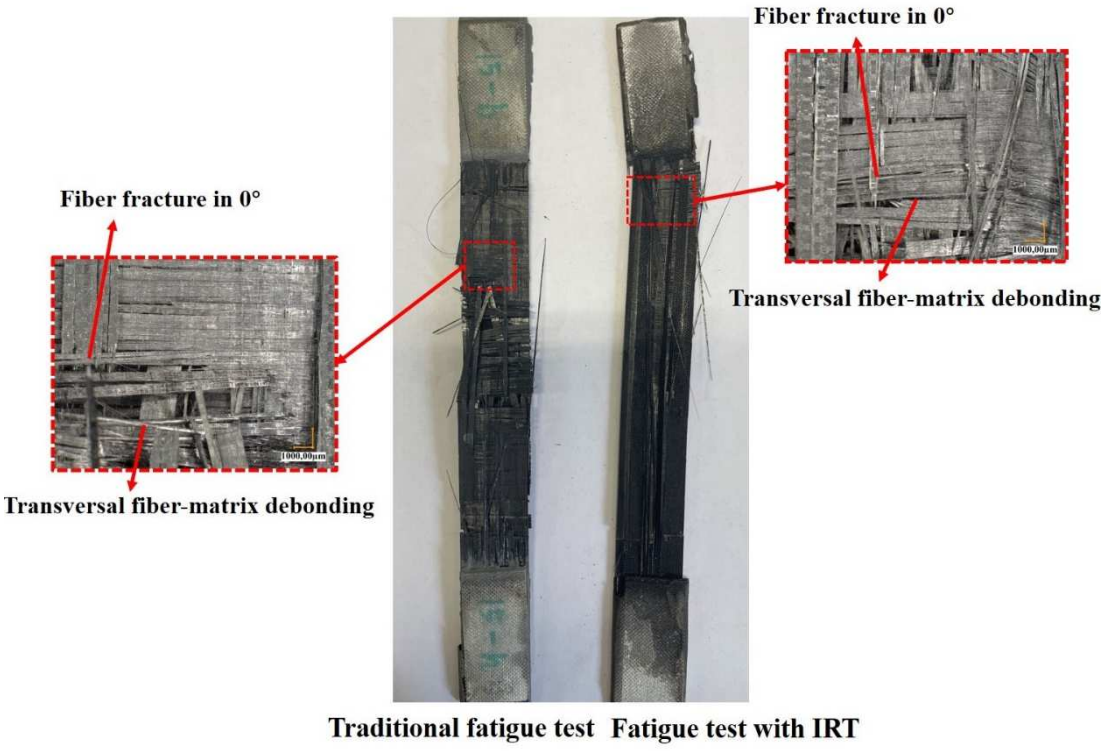

(a)

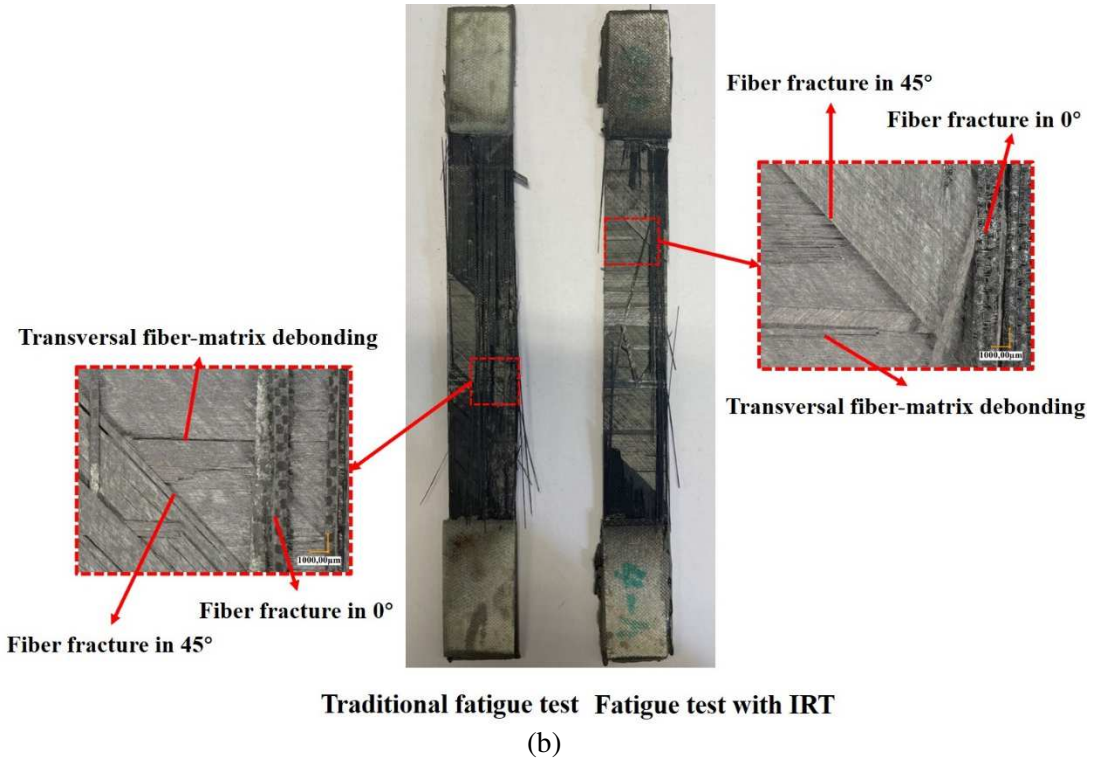

(b)

Fig. 16 Observation on fracture surfaces of the specimens after two types of fatigue tests: (a) QI laminates; (b) cross-ply laminates

4.2 Determination of S-N curves

Based on the study of two cases, it can be found that the S-N curves corresponding to $N_{fl} = 10^6$ cycles are lower than the traditional fatigue test results for both MD CFRP laminates,

while the curves corresponding to $N_{fl} = 10^7$ cycles lie within the 95% confidence interval. The fatigue life (number of cycles) corresponding to the fatigue limit determined by the graphic methods based on thermographic data cannot be defined in the Luong and Risitano's methods [28][25]. In the engineering design processes, 10^6 to 10^7 cycles are usually considered as conventional fatigue life for most materials [59]. In the literature, almost all the validations of these methods are carried out by comparing the fatigue limits obtained by traditional fatigue tests between $N_{fl} = 10^6$ and 10^7 cycles whatever the materials tested. Therefore, in the step 3, the failure threshold stiffness was calculated when $N_{fl} = 10^6$ and 10^7 cycles. The results of two MD CFRP laminates imply that the S-N curves corresponding to $N_{fl} = 10^6$ cycles are relatively more conservative, while those corresponding to $N_{fl} = 10^7$ cycles match well with the traditional fatigue test results.

Even though both Huang's model and the modified model allow to determine the fatigue life in a short time, it is obvious that the S-N curves determined by the modified model are more reliable compared to Huang's model. For example, for the QI laminates, when the maximum stress is 75% UTS, the corresponding fatigue life determined by traditional S-N curve is 942275 cycles. The fatigue life corresponding to $N_{fl} = 10^6$ and 10^7 cycles determined by Huang's model are 14421 and 144211 cycles, respectively, while those determined by the modified model are 61317 and 613192 cycles, respectively. However, it should be noted that the modified model was only verified by two kinds of MD CFRP laminates in this work. It is certain that more experimental data (other types of MD stacking sequences, composite materials, under other fatigue modes, etc.) are necessary to demonstrate the applicability of modified model to all kinds of MD laminates and also, to clarify the physical damage related to the parameter *r*.

5 Conclusions

In this work, the fatigue life prediction model proposed by Huang et al. [44] has been modified. A new parameter *r* is introduced into original expression of normalized stiffness to take the more complex damage mechanisms in the MD CFRP laminates into account. In addition, the stabilized temperature rise is normalized by the maximum value reached for the ease of comparison between different specimens. In order to validate this modified model, the experimental data of two different types of MD CFRP laminates, cross-ply and QI laminates, were used in the present work. Through the work of this study, the following conclusions can be drawn:

a) In the static tensile tests, QI laminates failed in a combination of transversal fiber-matrix debonding in 90° and $\pm 45^\circ$ layers, fiber fracture in $\pm 45^\circ$ and 0° layers and fiber pull-out in the surface 0° layers. While in the cross-ply laminates, the failure mode is characterized by a mixture of fiber fracture in the 0° layers along with transversal fiber/matrix debonding in the 90° layers.

b) There is a little difference in fracture surfaces between the traditional fatigue test specimens and those who have been subjected to step-loading procedure using IRT. The fracture surfaces of fatigue test specimens look similar to those of static test specimens except that the fiber fracture in the interior -45° layers was not observed in the fatigue test specimens.

c) The results have shown that the modified model proposed in this study allows to

determine correctly the S-N curves of QI and cross-ply CFRP laminates tested. In particular, although their S-N curves corresponding to $N_{fl} = 10^6$ cycles are shown conservative compared to those from the traditional fatigue test results, the maximum safety factor is no more than 1.15 for the two tested materials. Whereas the S-N curves corresponding to $N_{fl} = 10^7$ cycles lie totally within the 95% confidence intervals of traditional fatigue test results.

d) The modified model proposed in this study is more general than Huang's model. It allows to determine the S-N curve of a multidirectional composite just in about ten hours of testing machine time instead of one month and a half by using traditional fatigue tests.

e) Even though the modified model proposed in this paper need to be confirmed by much more experimental data (other types of MD stacking sequences, composite materials, under other fatigue modes, etc.), it has proven to be a reliable and promising way to determine rapidly the fatigue life of QI and cross-ply CFRP laminates and it should have a larger application scope.

Acknowledgements

The author Zijiao Jia was supported by China Scholarship Council (CSC) for three years PhD study at the University of Toulouse.

References

[1] Xian G, Guo R, Li C, Wang Y. Mechanical performance evolution and life prediction of prestressed CFRP plate exposed to hygrothermal and freeze-thaw environments. Composite Structures, 2022, 293: 115719.

[2] Tai N H, Ma C C M, Wu S H. Fatigue behaviour of carbon fibre/PEEK laminate composites. Composites, 1995, 26(8): 551-559.

[3] Konur O, Matthews F L. Effect of the properties of the constituents on the fatigue performance of composites: a review. Composites, 1989, 20(4): 317-328.

[4] Hiremath C, Senthilnathan K, Guha A, Tewari A. Effect of volume fraction on damage accumulation for a lattice arrangement of fibers in CFRP. Materials Today: Proceedings, 2015, 2(4-5): 2671-2678.

[5] Talreja R. Fatigue of composite materials: damage mechanisms and fatigue-life diagrams. Proceedings of the Royal Society of London A. Mathematical and Physical Sciences, 1981, 378(1775): 461-475.

[6] Fargione G, Giudice F, Risitano A. The influence of the load frequency on the high cycle fatigue behaviour. Theoretical and Applied Fracture Mechanics, 2017, 88: 97-106.

[7] Mohammadi B, Fazlali B. Off-axis fatigue behaviour of unidirectional laminates based on a microscale fatigue damage model under different stress ratios. International Journal of Fatigue, 2018, 106: 11-23.

[8] Lopes H P, Elias C N, Vieira M V B, Vieira V T, de Souza L C, Dos Santos A L. Influence of surface roughness on the fatigue life of nickel-titanium rotary endodontic instruments. Journal of Endodontics, 2016, 42(6): 965-968.

[9] Bagehorn S, Wehr J, Maier H J. Application of mechanical surface finishing processes for roughness reduction and fatigue improvement of additively manufactured Ti-6Al-4V

parts. International Journal of Fatigue, 2017, 102: 135-142.
[10] Brunbauer J, Pinter G. Effects of mean stress and fibre volume content on the fatigue-induced damage mechanisms in CFRP. International Journal of Fatigue, 2015, 75: 28-38.
[11] Brunbauer J, Stadler H, Pinter G. Mechanical properties, fatigue damage and microstructure of carbon/epoxy laminates depending on fibre volume content. International Journal of Fatigue, 2015, 70: 85-92.
[12] Gamstedt E K, Talreja R. Fatigue damage mechanisms in unidirectional carbon-fibre-reinforced plastics. Journal of Materials Science, 1999, 34(11): 2535-2546.
[13] Dong H, Li Z, Wang J, Karihaloo B L. A new fatigue failure theory for multidirectional fiber-reinforced composite laminates with arbitrary stacking sequence. International Journal of Fatigue, 2016, 87: 294-300.
[14] Vedrtnam A. Novel method for improving fatigue behavior of carbon fiber reinforced epoxy composite. Composites Part B: Engineering, 2019, 157: 305-321.
[15] Large-Toumi B, Salvia M, Vincent L. Fiber-matrix interface effect on monotonic and fatigue behavior of unidirectional carbon/epoxy composites, fiber, matrix, and interface properties. ASTM International, 1996, 1290: 182-200.
[16] Wu J, Lan C, Xian G, Li H. Recognition of damage pattern and evolution in CFRP cable with a novel bonding anchorage by acoustic emission. Smart structures and systems, 2018, 21(4): 421-433.
[17] Li C, Guo R, Xian G, Li H. Effects of elevated temperature, hydraulic pressure and fatigue loading on the property evolution of a carbon/glass fiber hybrid rod. Polymer Testing, 2020, 90: 106761.
[18] Huang Y, Li S X, Lin S E, Shih C N. Using the method of infrared sensing for monitoring fatigue process of metals. Materials Evaluation, 1984, 42(8).
[19] Jiang L, Wang H, Liaw P K, Brooks C R, Klarstrom D L. Characterization of the temperature evolution during high-cycle fatigue of the ULTIMET superalloy: experiment and theoretical modeling. Metallurgical and Materials Transactions A, 2001, 32(9): 2279.
[20] Jiang L, Wang H, Liaw P K, Brooks C R, Chen L, Klarstrom D L. Temperature evolution and life prediction in fatigue of superalloys. Metallurgical and Materials Transactions A, 2004, 35(3): 839-848.
[21] Yang B, Liaw P K, Wang G, Morrison M, Liu C T, Buchanan R A, Yokoyama Y. In-situ thermographic observation of mechanical damage in bulk-metallic glasses during fatigue and tensile experiments. Intermetallics, 2004, 12(10-11): 1265-1274.
[22] Curà F, Curti G, Sesana R. A new iteration method for the thermographic determination of fatigue limit in steels. International Journal of Fatigue, 2005, 27(4): 453-459.
[23] Amiri M, Khonsari M M. Life prediction of metals undergoing fatigue load based on temperature evolution. Materials Science and Engineering: A, 2010, 527(6): 1555-1559.
[24] Amiri M, Khonsari M M. Rapid determination of fatigue failure based on temperature evolution: Fully reversed bending load. International Journal of Fatigue, 2010, 32(2): 382-389.
[25] La Rosa G, Risitano A. Thermographic methodology for rapid determination of the fatigue limit of materials and mechanical components. International Journal of Fatigue, 2000, 22(1): 65-73.
[26] Fargione G, Risitano A. Rapid determination of the fatigue curve by the thermographic

method. International Journal of Fatigue, 2002, 24: 11−19.
[27] Luong M P. Fatigue limit evaluation of metals using an infrared thermographic technique. Mechanics of Materials, 1998, 28(1-4): 155-163.
[28] Luong M P. Infrared thermographic scanning of fatigue in metals. Nuclear Engineering and Design, 1995, 158(2-3): 363-376.
[29] Colombo C, Libonati F, Pezzani F, Salerno A, Vergani L. Fatigue behaviour of a GFRP laminate by thermographic measurements. Procedia Engineering, 2011, 10: 3518-3527.
[30] Peyrac C, Jollivet T, Leray N, Lefebvre F, Westphal O, Gornet L. Self-heating method for fatigue limit determination on thermoplastic composites. Procedia Engineering, 2015, 133: 129-135.
[31] Montesano J, Fawaz Z, Bougherara H. Use of infrared thermography to investigate the fatigue behavior of a carbon fiber reinforced polymer composite. Composite Structures, 2013, 97: 76-83.
[32] Jiang L, Wang H, Liaw P K, Brooks C R, Chen L, Klarstrom D L. Temperature evolution and life prediction in fatigue of superalloys. Metallurgical and Materials Transactions A, 2004, 35(3): 839-848.
[33] Amiri M, Khonsari M M. Rapid determination of fatigue failure based on temperature evolution: Fully reversed bending load. International Journal of Fatigue, 2010, 32(2): 382-389.
[34] Liakat M, Khonsari M M. Analysis and life prediction of a composite laminate under cyclic loading. Composites Part B: Engineering, 2016, 84: 98-108.
[35] Van Paepegem W, Degrieck J. Coupled residual stiffness and strength model for fatigue of fibre-reinforced composite materials. Composites Science and Technology, 2002, 62(5): 687-696.
[36] Talreja R. Multi-scale modeling in damage mechanics of composite materials. Journal of materials science, 2006, 41(20): 6800-6812.
[37] Jamison R D, Reifsnider K L, Schulte K, Stinchcomb W W. Characterization and analysis of damage mechanisms in tension-tension fatigue of graphite/epoxy laminates. Effects of Defects in Composite Materials, ASTM International, 1984, 21-55.
[38] Shokrieh M M, Lessard L B. Multiaxial fatigue behaviour of unidirectional plies based on uniaxial fatigue experiments - II. Experimental evaluation. International Journal of Fatigue, 1997, 19(3): 209-217.
[39] Shiri S, Yazdani M, Pourgol-Mohammad M. A fatigue damage accumulation model based on stiffness degradation of composite materials. Materials & Design, 2015, 88: 1290-1295.
[40] Senthilnathan K, Hiremath C P, Naik N K, Guha A, Tewari A. Microstructural damage dependent stiffness prediction of unidirectional CFRP composite under cyclic loading. Composites Part A: Applied Science and Manufacturing, 2017, 100: 118-127.
[41] Peng T, Liu Y, Saxena A, Goebel K. In-situ fatigue life prognosis for composite laminates based on stiffness degradation. Composite Structures, 2015, 132: 155-165.
[42] Whitworth H A. A stiffness degradation model for composite laminates under fatigue loading. Composite Structures, 1997, 40(2): 95-101.
[43] Tang R, Guo Y J, Weitsman Y J. An appropriate stiffness degradation parameter to monitor fatigue damage evolution in composites. International Journal of Fatigue, 2004,

26(4): 421-427.
[44] Huang J, Pastor M L, Garnier C, Gong X. A new model for fatigue life prediction based on infrared thermography and degradation process for CFRP composite laminates. International Journal of Fatigue, 2019, 120: 87-95.
[45] Huang J, Garnier C, Pastor M L, Gong X. Investigation of self-heating and life prediction in CFRP laminates under cyclic shear loading condition based on the infrared thermographic data. Engineering Fracture Mechanics, 2020, 229: 106971.
[46] ISO 527-4:2021, Plastics - Determination of tensile properties - Part 4: Test conditions for isotropic and orthotropic fibre-reinforced plastic composites, 2021.
[47] Lemma E, Chen L, Siores E, Wang J. Study of cutting fiber-reinforced composites by using abrasive water-jet with cutting head oscillation. Composite structures, 2002, 57(1-4): 297-303.
[48] Ferri O M, Ebel T, Bormann R. Influence of surface quality and porosity on fatigue behaviour of Ti–6Al–4V components processed by MIM. Materials Science and Engineering: A, 2010, 527(7-8): 1800-1805.
[49] ASTM, D 3479/D 3479M–96. Standard test method for tension–tension fatigue of polymer matrix composite materials. ASTM, International, 2007.
[50] ASTM D 3039/D 3039M-08. Standard test method for tensile properties of polymer matrix composite materials. ASTM, International, 2014.
[51] Parmiggiani A, Prato M, Pizzorni M. Effect of the fiber orientation on the tensile and flexural behavior of continuous carbon fiber composites made via fused filament fabrication. The International Journal of Advanced Manufacturing Technology, 2021, 114: 2085-2101.
[52] Li X, Saeedifar M, Benedictus R, Zarouchas D. Damage accumulation analysis of cfrp cross-ply laminates under different tensile loading rates. Composites Part C: Open Access, 2020, 1: 100005.
[53] Stinchcomb W W, Bakis C E. Fatigue behavior of composite laminates, Composite Materials series, 1991, 4: 105-180.
[54] Alam P, Mamalis D, Robert C, Floreani C, Brádaigh C M Ó. The fatigue of carbon fibre reinforced plastics-A review. Composites Part B: Engineering, 2019, 166: 555-579.
[55] Godines C, DorMohammadi S, Abdi F, Villa Montero M, Huang D, Minnetyan L. Damage tolerant composite design principles for aircraft components under static service loading using multi-scale progressive failure analysis. Composite Materials, 2017, 51(10): 1393-1419.
[56] Vasiukov D, Panier S, Hachemi A. Direct method for life prediction of fibre reinforced polymer composites based on kinematic of damage potential. International Journal of Fatigue, 2015, 70: 289-296.
[57] Mao H, Mahadevan S. Fatigue damage modelling of composite materials. Composite Structures, 2002, 58(4): 405-410.
[58] Jia Z, Pastor M L, Garnier C, Gong X. A new method for determination of fatigue limit of composite laminates based on thermographic data. International Journal of Fatigue, 2023, 168: 107445.
[59] Bathias C. There is no infinite fatigue life in metallic materials. Fatigue & fracture of

1 engineering materials & structures (Print), 1999, 22(7): 559-565.